ARC ELECTRODE INTERACTION STUDY

Final report for NASA Grant
NASA/NAG3-1332

submitted to

Mr. Charles Sarmiento
Program Monitor
NASA Lewis Research Center

by

X. Zhou, D. Berns, and J. Heberlein
High Temperature Laboratory
Department of Mechanical Engineering
University of Minnesota
Minneapolis, MN 55455

January 31, 1994.

ARC ELECTRODE INTERACTION STUDY

1. OVERVIEW

The project consisted of two parts: (1) the cathode interaction studies which were a continuation of previous work and had the objective of increasing our understanding of the microscopic phenomena controlling cathode erosion in arcjet thrusters, and (2) the studies of the anode attachment in arcjet thrusters. The cathode interaction studies consisted of (a) a continuation of some modeling work in which the previously derived model for the cathode heating was applied to some specific gases and electrode materials, and (b) experimental work in which various diagnostics was applied to the cathode. The specific diagnostics used were observation of the cathode tip during arcing using a Laser Strobe Video system in conjunction with a tele-microscope, a monochromator with an optical multichannel analyzer for the determination of the cathode temperature distribution, and various ex situ materials analysis methods. The emphasis of our effort was shifted to the cathode materials analysis because a parallel project was in place during the second half of 1993 with a visiting scientist pursuing arc electrode materials studies. As a consequence, the diagnostic investigations of the arc in front of the cathode had to be postponed to the first half of 1994, and we are presently preparing these measurements. The results of last year's study have shown some unexpected effects influencing the cathode erosion behavior, such as increased erosion away from the cathode tip, and our understanding of these effects should improve our ability to control cathode erosion.

The arcjet anode attachment studies concentrated on diagnostics of the instabilities in subsonic anode attachment arcjet thrusters, and were supplemental measurements to work which was performed by one of the authors (D. Berns) who spent the summer as an intern at NASA Lewis Research Center. This report includes a summary of the results obtained during the internship because they formed an integral part of the study. We are preparing two tasks for 1994, the diagnostics of the anode closure phenomenon, and the use of arcjet thrusters for the deposition of c-BN.

2. CATHODE EROSION STUDIES

2.1 Research Objectives

Insufficient electrode life and uncertainties in that life are major problems hampering the development in many plasma application areas which make use of plasma torches, arc heaters, and arc jet thrusters. In spite of a considerable amount of work published dealing with arc-cathode phenomena, our present understanding is still incomplete because different physical phenomena dominate for different combinations of experimental parameters [1, 2].

The objective of our present research project is to gain a better understanding of the behavior of arc-cathode surface interaction over a wide range of parameters, and furthermore to develop guidelines for better design of the electrode and the selection of materials. Both, modeling and experimental diagnostics are being used to identify the dominant microscopic processes responsible for the cathode material loss.

2.2 Theoretical Research.

We have previously reported results of a theoretical study which predicted that high current arc cathode erosion is predominantly dependent on the work function and the vapor pressure of the cathode material, and that the thermal design plays a secondary role. These results have been obtained with a newly developed self-consistent model of the cathode region including a realistic one-dimensional sheath model. The results have been obtained for an argon arc and a tungsten cathode [3].

The model has now been extended and results have been obtained for different arc gases and different electrode materials. The arc gas has a strong effect because it affects not only the temperature at the boundary between the arc and the cathode region, but also the electron density in the cathode region and at the cathode.

The results of the calculations show that the cathode material plays a dominant role in terms of the cathode spot temperature and the associated mass loss rate by evaporation of cathode material. Since the addition of thorium oxide to tungsten reduces the work function of the cathode material, the cathode spot temperature as well as the mass loss rate by evaporation are reduced. For the same cathode material, hydrogen leads to the highest cathode spot temperature and mass loss rate, followed by nitrogen and argon. The current density at the cathode spot, the cathode spot size, and the percentages of the energy fluxes removed from the cathode spot are mainly determined by the plasma gas rather than by the cathode material.

The results were presented at the IEEE International Holm Conference in Pittsburgh, on September 27, 1993 [4].

2.3 Experimental Investigation

2.3.1 Insitu Observation of Thermionic Cathode Spot Behavior in Argon

An new in situ observation method has been applied to investigate the behavior of thermionic cathode spots in argon arcs. The insitu observation system includes a tele-microscope, a laser stroboscopic video camera, and a narrow band filter.

Different cathode materials and different cathode geometric shapes have been studied. For thoriated tungsten cathodes with a conical tip, our observations have shown that arcing will result in enhanced erosion at the edge of the arc spot (neck erosion), leading to a sudden loss of the cone tip and leaving a truncated cone (as shown in Fig.1). However, for pure tungsten cathodes, the original shape of the cathode tip is unimportant since the cathode spot will be in a molten state soon after arcing starts. The results also show that the cathode spot increases as the arc current increases for both thoriated tungsten and pure tungsten cathodes (as shown in Fig.2).

The results have been presented in an interim report to NASA during Mr. J. Sankovic's visit at the University of Minnesota in June, 1993.

2.3.2 Metallurgical Study of 2% Thoriated Tungsten Cathodes

This study was a cooperative effort with a visiting scientist, Prof. B. Ding, from Xi'an Jiaoton University, P.R. China.

The cathode assembly has been redesigned in order to allow a metallurgical study of the cathode spot erosion phenomena. Instead of being silver soldered onto the copper base, the thoriated tungsten or pure tungsten cathode tip is now clamped onto the copper base, which completely eliminates the influences of the soldering process on the heat balance and erosion measurements. SEM, EDX, and image analysis have been used to evaluate the cathode erosion.

Experimental conditions have been: four different arcing durations (5 minutes, 20 minutes, 40 minutes, and 60 minutes); a chamber pressure of 340 torr; argon as the working gas with a flow rate of 20 l/min. A copper anode nozzle has been used with a diameter of 3/16"; The diameter of the thoriated tungsten cathode has been 1/4".

Figure 3 shows that the neck erosion is beginning to appear at about 20 minutes after starting the arc, a value corroborated by our observation with the Laser Strobe Video system. From Fig. 4 we could deduce that as the arcing time increases, thoria is depleted at locations further away from the cathode spot surface. However, even after 60 minutes arcing, there is still thoria at the necking area. Rings of tungsten crystallites and of thorium crystallites have been found on the cathode surface outside of the cathode spot, and tungsten crystals also have been observed near the necking area at the cathode spot (as shown in Fig.5). Fig.6 shows how the porosity of the cathode spot surface increases with arcing time.

From this study and the cathode temperature distribution measurement, some conclusions have been obtained. At the cathode spot surface, the rate of evaporation of thoria is much faster than that of diffusion of thoria from the inside of the cathode. Since there are tungsten crystals and thorium crystals deposited from tungsten vapor and thorium vapor on the cathode surface outside of the cathode spot, there might be vapor transport by small gas vortices near the cathode tip, which has been predicted by a theoretical study [5]. The causes for the porosity of the cathode spot surface is not known yet. Zhukov [6] suggested that since the melting point of thoria is much lower than that of tungsten, vaporized thoria forms bubbles on a molten surface leading to the porous structure, however other investigators have hypothesized that vapor phase deposition of tungsten may occur. Further investigations need to be carried out.

2.3.3 Cathode Spot Temperature Measurement with the OMA System

The major problem with the cathode temperature distribution measurement is associated with the radiation from the plasma, the perturbation of the plasma characteristics by the measurement technique, or the inability to provide temperature measurements with sufficient spatial resolution in the area where the cathode temperature changes dramatically.

An OMA system has been successfully applied to measure the temperature distribution of the cathode surface. This OMA system has a CCD image sensor device which provides a matrix array of 512 by 512 solid state sensors. This gives us a very high spatial resolution (up to 19 μm).

Optical radiation from the arc and the cathode is imaged by a lens system on the entrance slit of a 0.5 meter monochromator with a magnification of 3:1 and detected with the OMA system at the monochromator exit. So the effective spatial resolution at the arc and the cathode is equal to an area of approximately 6 μm by 6 μm. The spectral response of the system is calibrated against a standard tungsten ribbon lamp.

A previous study [7] has shown that in the wavelength range above 900 nm, the continuum radiation from the plasma can be neglected compared with the radiation from the cathode surface. In order to eliminate the influence from the plasma radiation, our measurements have been taken in two infrared wavelength ranges at 820.42 nm to 821.82 nm and at 920.24 nm to 921.54 nm.

Both single color pyrometry and two color pyrometry have been used. Results are obtained from an average of 60 measurements at the same time. Due to the method itself and the characteristics of the CCD image sensor device, the results of two color pyrometry give a large statistical variation of up to 1000 K, while the results of single color pyrometry show only 20 K error. However, the average results of these two methods agree relatively well. Also, the measured temperature values obtained using single color pyrometry has been found to be the same when two different wavelength ranges were used. The emissivity values for tungsten were obtained from Yih and Wang [8].

Figure 7 shows that the temperatures at the cathode tip are almost the same for both 1/4" diameter and 1/8" diameter cathodes. There appears also only a relatively small difference between the cathode temperatures for a 150 A arc current and those for 200 A. The 1/8" diameter cathodes show higher temperatures away from the tip compared to the 1/4" diameter cathodes, because the heat loss due to heat conduction inside the cathode is higher for the 1/4" diameter cathode than that for the 1/8" diameter cathode.

The results indicate that the OMA system can provide good temperature distribution measurements at the cathode surface with single color pyrometry. Also the modeling results predicting little influence of the thermal design on the cathode spot temperature for arcing conditions as were used in these experiments have been verified.

2.4 Future Work

It is planned that the OMA system will be employed to measure the electron number densities in front of the cathode spot by using Stark broadening to allow derivation of current density values.

3. REVIEW OF SUBSONIC-ANODE-ATTACHMENT ARCJET THRUSTER TESTS

The work presented here was performed over the past year and a half at the University of Minnesota and during two summer internships at NASA Lewis Research Center. A general overview of all testing will be presented in the following paragraphs. This research has been the source for three conference papers and a Master's Thesis [9-12].

The motivation for the work presented follows the desire to gain a better understanding of plasma phenomena in arcjets. At the same time as the supersonic-anode-attachment arcjet designs were being developed in the 1960's, subsonic-anode-attachment arcjets (attachment of the arc along the subsonic, high pressure region of the anode/nozzle) were investigated [13-15]. These early subsonic-anode-attachment arcjets operated with higher efficiencies and about the same specific impulse values as their supersonic-anode-attachment counterparts but experienced arc voltage instabilities and higher anode heat losses. The focus of the research presented here was to determine if the subsonic-anode-attachment arcjet design had any merit as a higher performance thruster (greater performance than the conventional supersonic-anode-attachment designs) and more importantly, to measure the arc instabilities associated with this design and determine what effect these instabilities had on arcjet operation. The static pressure profiles through the nozzle were also measured to gain an understanding of flow effects in arcjet nozzles. Previous hydrogen arcjet testing at different power levels and with several different anode/nozzle designs were used as reference for this research [16-23].

Testing was performed at the University of Minnesota and at NASA Lewis Research Center. The vacuum facility at the University of Minnesota is shown if Figure 8. Two arcjets, a low and a medium power design, were operated with both a solid and a segmented nozzle (Figures 9 and 10). Testing began with the low power (0.5-2kW) arcjet by measuring arcjet performance with a solid anode. The arcjet was operated at various currents and propellant flowrates (Figure 11 shows the low power arcjet in operation). The thrust for the various operation levels was recorded along with an oscilloscope record of the arc voltage and current. The identification of arc instabilities led to the use of a segmented anode for further analysis of the arc. The segmented anode, which was made to the exact dimensions of the solid anode, was then used to measure the total arc voltage and the current flow to different sections of the anode.

Experiments continued with the medium power (5-10kW) arcjet. The goal of these tests was to determine whether the medium power subsonic-anode-attachment arcjet design would exhibit the same arc instabilities as seen with the low power arcjet and to

determine how the performance of the medium power arcjet would compare to other medium power arcjet designs. The larger dimensions of the medium power arcjet nozzle were also utilized for placement of multiple pressure taps along the walls of the anode body.

The solid anode design was used to determine the operation characteristics of the arcjet. The thruster was operated with various propellants and at various background pressures in the Minnesota facility. Photos of typical arcjet operation are shown in Figure 12. Only limited thrust data was obtainable due to complications between the arcjet and the starting circuit of the power supply.

The final stage of the testing was performed with a segmented anode in the medium power arcjet. The segmented anode thruster mounted in Tank 9 at NASA LeRC is shown in Figure 13. The frequency of the arc instabilities was tied to the variations in arc current and propellant flow rate while static pressure profiles along the arcjet nozzle were obtained and correlated with arc current, propellant flowrate, and background pressure.

For all arcjet configurations a high frequency voltage instability was identified and shown to be caused by arc restrike. The voltage stability of the low power design was strongly affected by current and propellant flowrate. Three operating regimes were identified. At low currents and flowrates the voltage was stable (maintained a relatively constant value). As either parameter was raised, the arc entered a transition zone characterized by periods of high frequency voltage oscillations caused by movement of the arc attachment point on the anode. Further increases in the current or flowrate caused the voltage oscillations to become continuous. Figure 14 is a typical oscilloscope record of the arc voltage and arc current for operation in the restrike mode.

The arc restrike cycle was shown to consist of an initial arc gap breakdown followed by an elongation of the arc column by downstream movement of the anode attachment point, and finally an arc restrike back to an initial upstream point. Two forces act on the arc anode attachment leg, a gasdynamic drag force which pushes the leg downstream and a Lorentz force which tends to counteract the drag force. Approximate calculations have shown, for these anode designs, that the drag force is about 4 times stronger than the electromagnetic force. Therefore, after an initial arc breakdown, the arc attachment leg is pushed downstream very quickly by the drag force until the voltage drop between the electrodes is large enough to overcome the breakdown voltage of the fringe gas between the arc column and the anode wall, at which time the arc restrikes to a position upstream and the cycle repeats. The movement of the arc root during restrike

was quantified by obtaining data for arc current contribution to the individual segments of both the low power and medium power segmented anodes. Figure 15 is a typical segmented anode oscilloscope record showing the restrike phenomenon.

For all operating conditions where restrike occurred, the anode attachment remained in the subsonic region of the nozzle. Variations in propellant flowrate and arc current had an effect on the behavior of the restrike phenomenon. For a constant current, increasing the flowrate pushes the arc attachment position farther downstream on the anode, this lengthening of the arc causes an increase in total average arc voltage, and forces a decrease in restrike frequency. For a constant flowrate, increasing the arc current causes a widening of the arc column. With a wider, less constricted arc column, the average arc voltage decreases. A decrease in breakdown voltage between the arc column and the anode wall, caused by the widened arc column (smaller gap and hotter fringe gas), forces an increase in restrike frequency.

The ability to control the position of the arc attachment by electrical switching of the anode segments was illustrated. Forcing the arc out of restrike was achieved along with stepping the arc root to different positions downstream of the anode.

Pressure profiles along the medium power nozzle were obtained for various flowrates and arc currents. Figure 16 shows the nozzle pressure profiles for both constant flowrate and constant current operation (the curves through the data points only serve to illustrate the trends, they are not based on any calculations). The gas static pressures were seen to increase with both flowrate and current. Static pressure of the flow through the nozzle increased with an increase in current at a fixed mass flow rate, and increased with an increase in mass flow rate for a fixed arc current. The exact mechanism by which the static pressure increase occurs in these high temperature gas flows can not be fully understood without the aid of a numerical fluid and thermodynamic model for the flow.

The interior nozzle pressures were shown to decrease continually through the nozzle suggesting that no shock formation existed within the nozzle for operation at background pressures below 1.5 torr. Isentropic expansion curves were fit to the experimental data with only small deviations, which suggests that even with heated flow, the gas flow through the nozzle can be roughly characterized by the isentropic case. Using the values of the restrike frequency, the position of the anode attachment, the nozzle pressures, and the mass flowrate, it is possible to obtain rough estimates of the bulk gas temperature and velocity inside of the arcjet nozzle.

At a given specific power level, specific impulse increased asymptotically with flowrate. At a given specific impulse, the thruster efficiency also increased asymptotically with flowrate. The subsonic anode attachment thruster operated radically

different than conventional designs. For a thruster which was not optimized, the performance was found to be below that of existing designs.

The arc stability of the low power arcjet was dependent on background pressure. The nature of the arc fluctuations was different for two background pressure levels of 18 Pa and .05 Pa. The reason for the arc voltage differences between arcjet operation in different background pressures is unclear.

From these experiments, a good understanding of the macroscopic physical behavior of the plasma flow through the subsonic-anode-attachment arcjets for various operation levels was obtained. It is expected that the acquired data in these tests and the experimental procedure used can be extended to gain a better understanding of arc instabilities and the physical operation of other arcjet designs and related plasma sources. It was shown that the high pressure anode attachment position and the arc restrike behavior make this type of anode resilient to high currents and very adjustable in operation. This type of nozzle could have potential for application in the area of materials processing. Arcjets are sources of high energy, supersonic plasma flows which are excellent environments for chemical reactions. The ability to adjust the operation parameters of the arcjet will allow control over the plasma properties in the arcjet plume, thereby changing the chemically reactive environment and improving control over chemical synthesis of materials from injected precursors. The arcjet thruster has many properties which make it attractive as a new plasma source for applications other than propulsion.

REFERENCES

1. A.E. Guile, "Arc-electrode phenomena", Proc. IEE, IEE Review, **118**(9), p.1131, 1971
2. W. Finkelnburg and H. Maecker, "Electric arcs and thermal plasma", Handbuch der Physik, **22**, p.256, 1956
3. X. Zhou, J. Heberlein, E. Pfender, "Theoretical study of factors influencing arc erosion of cathode", Proc. of the 38th Holm Conference on Electric Contacts, 1992
4. X. Zhou, J. Heberlein, E. Pfender, "Model predictions of arc cathode erosion rate dependence on plasma gas and on cathode material", Proc. of the 39th Holm Conference on Electric Contacts, 1993
5. P.C. Huang, Ph.D. Thesis, University of Minnesota, 1993

6. M.F. Zhukov, "Mass transfer at thermionic arc cathodes", Contrib. Plasma Phys., 29(3), p.315, 1989

7. O. Loesener, "Spektrale Charakterisierung des im Plasmawindkanal Lichtbogenbeheizten Luftgemischs fur Pyrometrische Zwecke", Internal Report, IRS-89-1B3, 1989

8. S. Yih and C. Wang, "Tungsten", Plenum Press, New York, 1979

9. Berns, D.H., "Investigation of Arc Instabilities In and Performance of Subsonic-Anode-Attachment Arcjet Thrusters," *Master of Science Thesis*, University of Minnesota, 1994.

10. Sankovic, J.M. and Berns, D.H., "Performance of a Low-Power Subsonic-Arc-Attachment Arcjet Thruster," AIAA 93-1898, June 1993.

11. Berns, D.H. and Sankovic, J.M., "Investigation of a Subsonic-Arc-Attachment Thruster Using Segmented Anodes," AIAA 93-1899, June 1993.

12. Berns, D.H., Heberlein, J., and Sankovic, J.M., "Internal Nozzle Parameters and Operation of a Subsonic-Anode-Attachment Medium Power Arcjet," submitted to *Joint Propulsion Conference*, June 1994.

13. John, R.R., "Thirty-Kilowatt Plasmajet Rocket Engine Development," Summary Report on the Second Year Development Program, Avco Corp, RAD-TR-64-6, (also NASA CR-54044), July 1964.

14. Todd, J.P. and Sheets, R.E., "Development of a Regeneratively Cooled 30-kW Arcjet Engine," *AIAA Journal*, Vol. 3, No. 1, pp. 122-126, 1965.

15. McCaughey, O.J., *et al.*, "Research and Advanced Development of a 2 kW Arc-Jet Thruster," Summary Report, Plasmadyne Corp., NASA CR-54035, June 1964.

16. Sankovic, J.M., *et al.*, "Hydrogen Arcjet Technology," IEPC 91-018, *Proceedings of the 22nd International Electric Propulsion Conference*, (also NASA TM 105340), October 1991.

17. Curran, F.M. and Haag, T.W., "Extended Life and Performance Test of a Low-Power Arcjet," *Journal of Spacecraft and Rockets*, Vol. 29, No. 4, pp. 444-452, July 1992.

18. Haag, T.W. and Curran, F.M., "High-Power Hydrogen Arcjet Performance," AIAA 91-2226, (also NASA TM105143), June 1991.

19. Curran, F.M., *et al.*, "Performance Characterization of a Segmented Anode Arcjet Thruster," AIAA 90-2582, (also NASA TM 103227), July 1990.

20. "H2 Arcjet Performance Mapping Program," Rocket Research Co. Report 92-R-1615 (also NASA CR 191073), January 1992.

21. Haag, T.M., "Recent Testing of 30-kW Hydrogen Arcjet Thrusters," AIAA 93-1902, June 1993.
22. Curran, F.M., *et al., "Medium* Power Hydrogen Arcjet Performance," AIAA 91-2227, (also NASA TM 104533), June 1991.
23. Sankovic, J.M. and Curran, F.M., "Arcjet Thermal Characteristics," AIAA 91-2456, (also NASA TM 105156), June 1991.

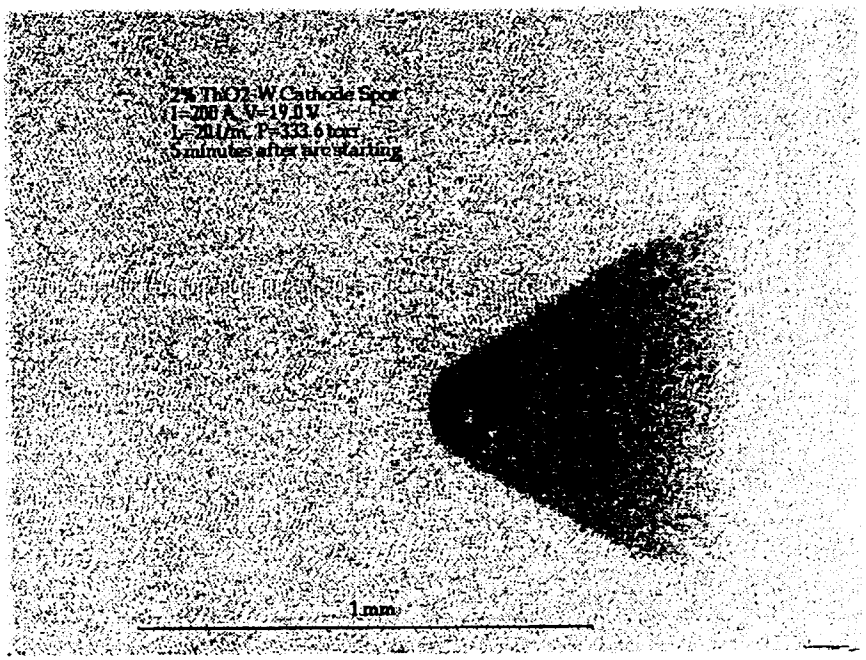

a)

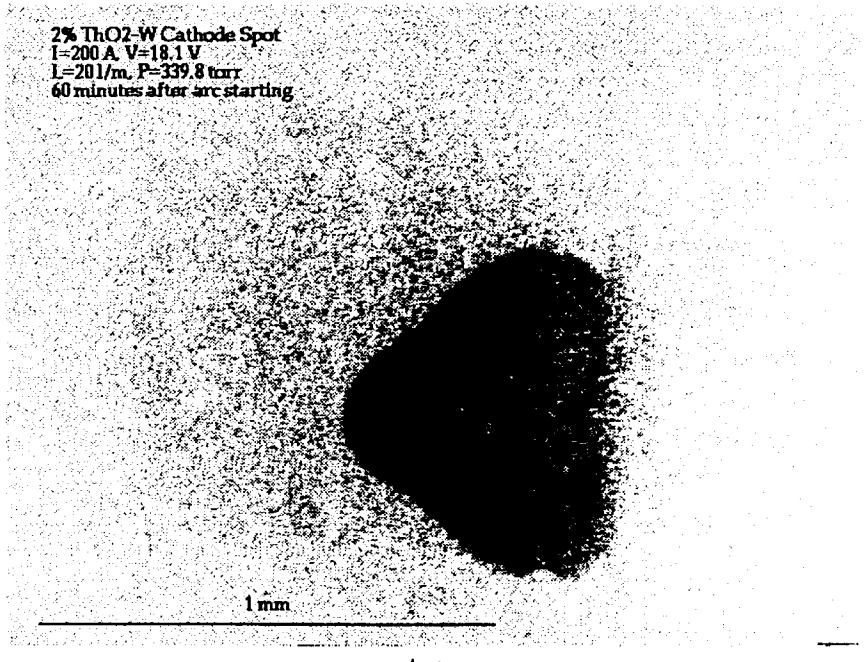

b)

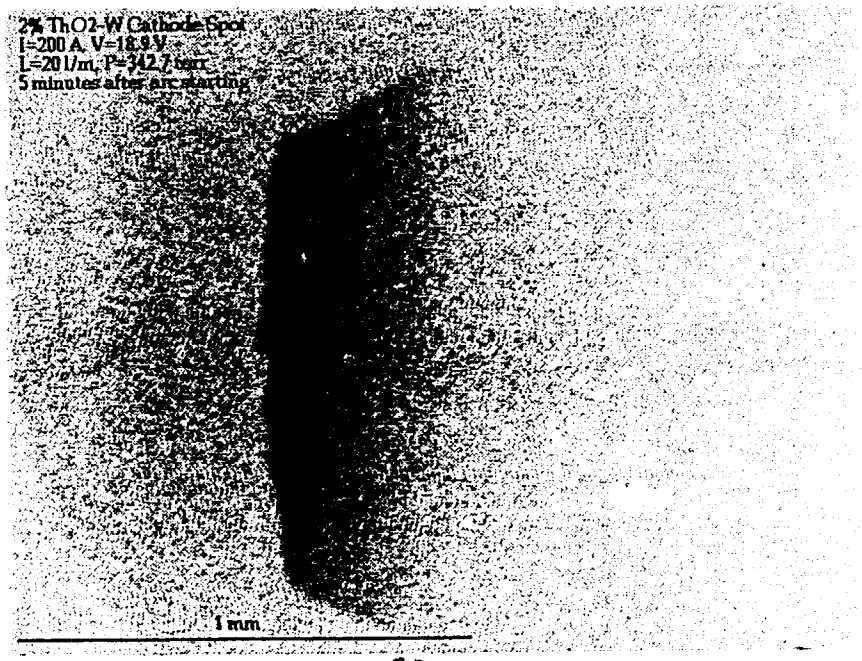

c)

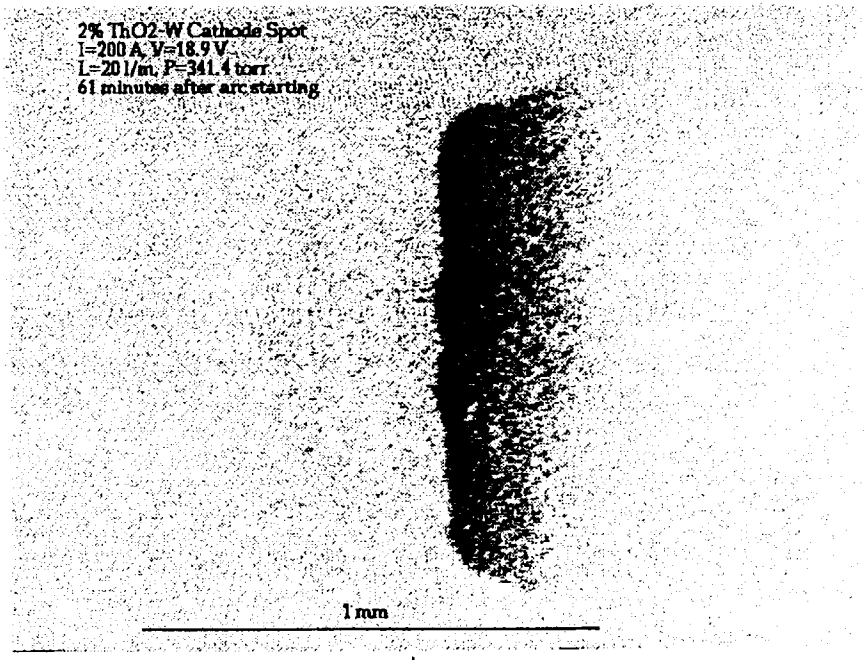

d)

Fig.1 2% thoriated tungsten cathode spot images with Ar arc at 335 torr: a) 5 minutes after arc starting for a cone shape cathode. b) 60 minutes after arc starting for a cone shape cathode. c) 5 minutes after arc starting for truncated cathode. d) 60 minutes after arc starting for truncated cathode.

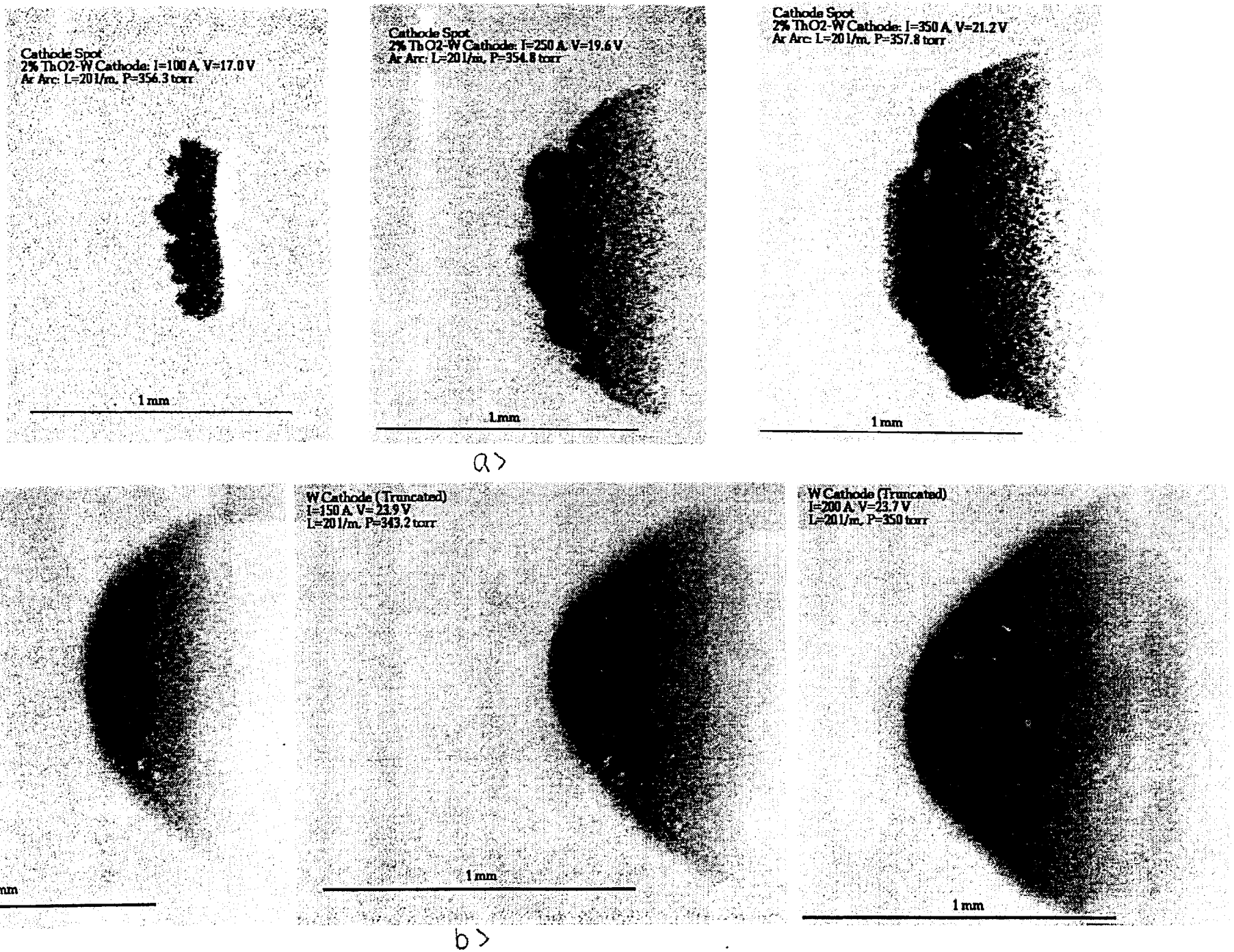

Fig.2 Cathode spot size increases as arc current increases. a) the cathode spot of thoriated tungsten cathode at different arc currents. b) the cathode spot of pure tungsten cathode at different arc currents.

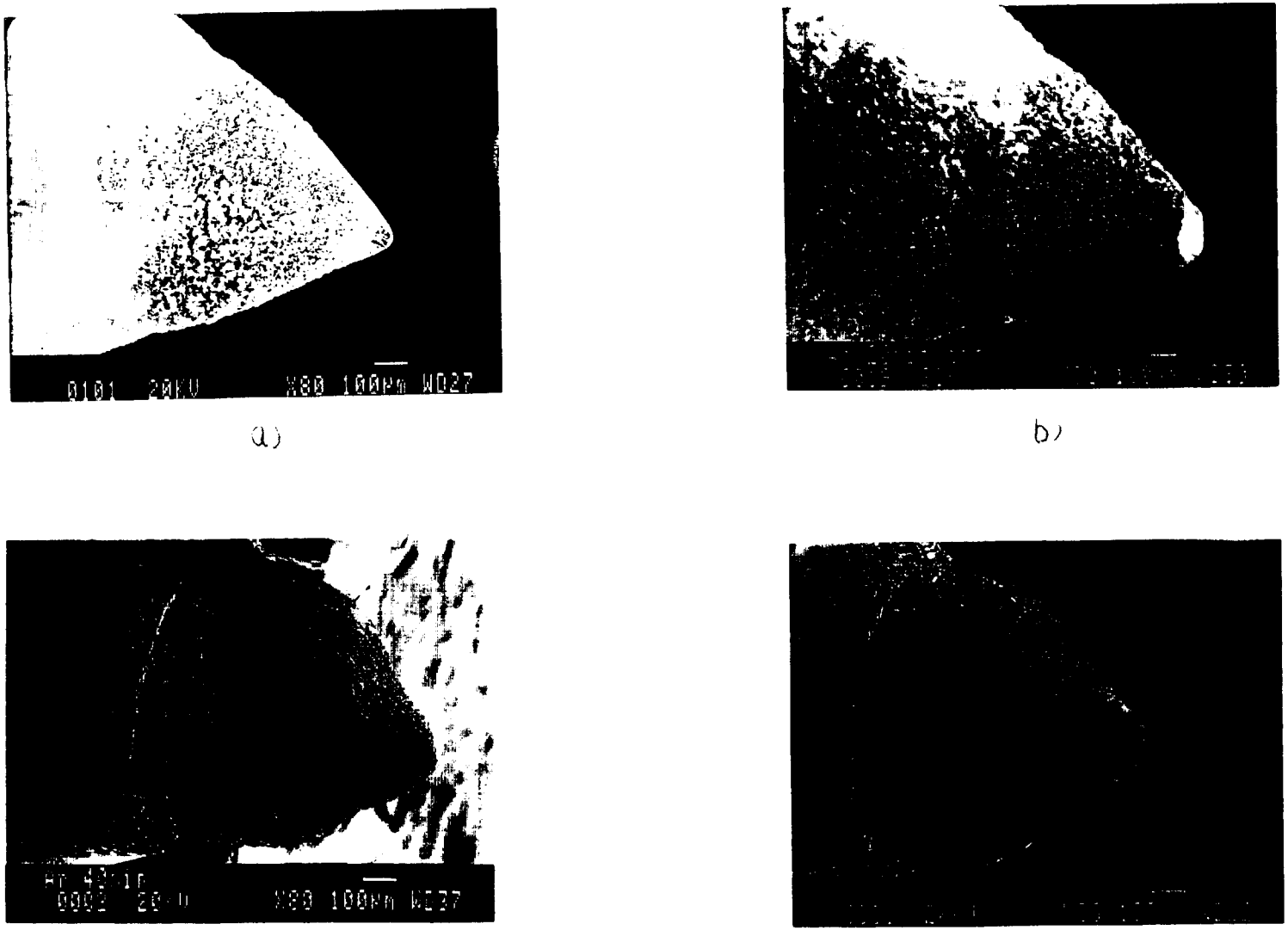

Fig.3 SEM photos of thoriated tungsten cathode tips. a) after 5 minutes arcing. b) after 20 minutes arcing. c) after 40 minutes arcing. d) after 60 minutes arcing.

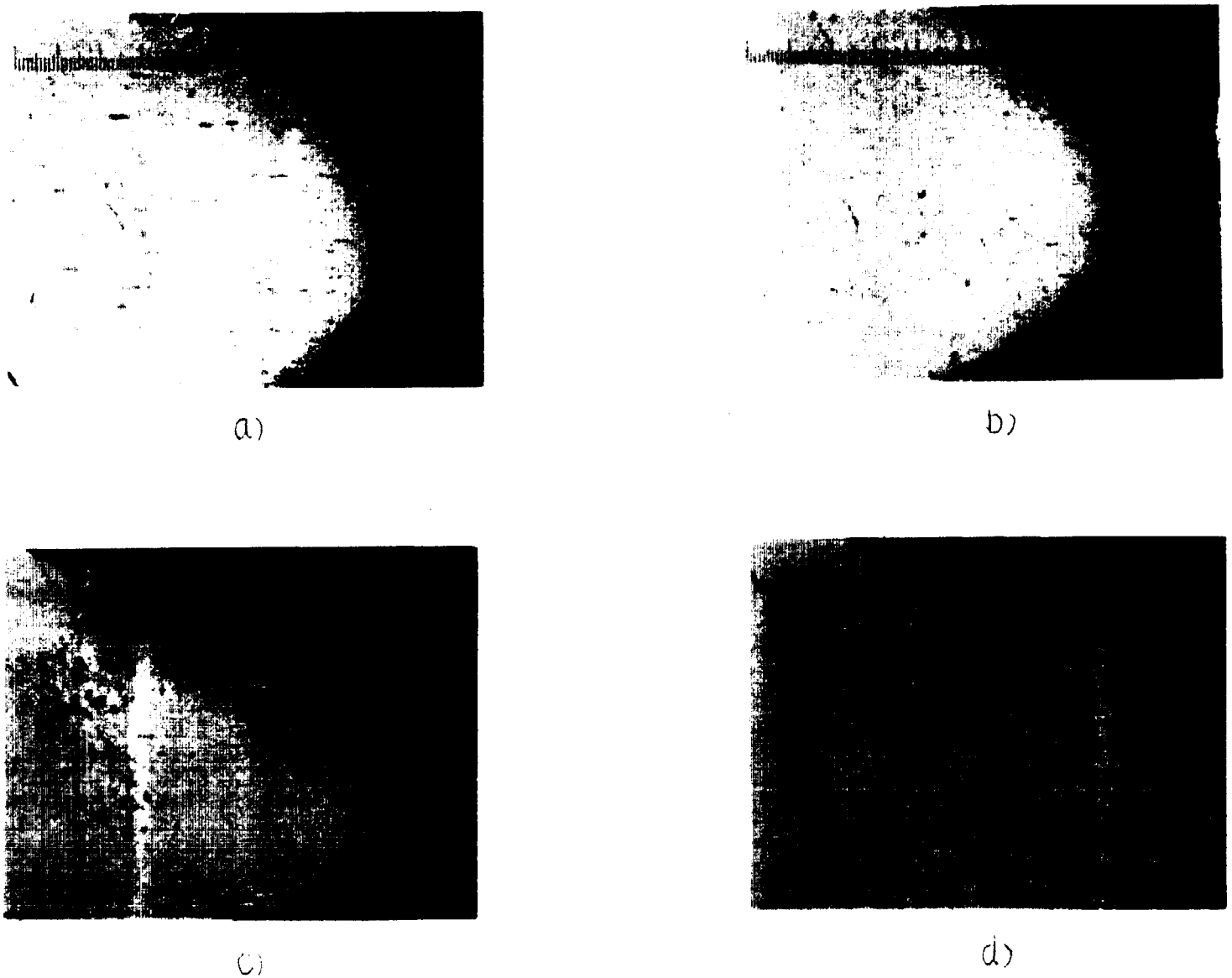

Fig.4 Electronic microscopic photos (x200) of polished cross sections of the cathode tips. a) 5 minutes after arcing. b) 20 minutes after arcing. c) 40 minutes after arcing. d) 60 minutes after arcing.

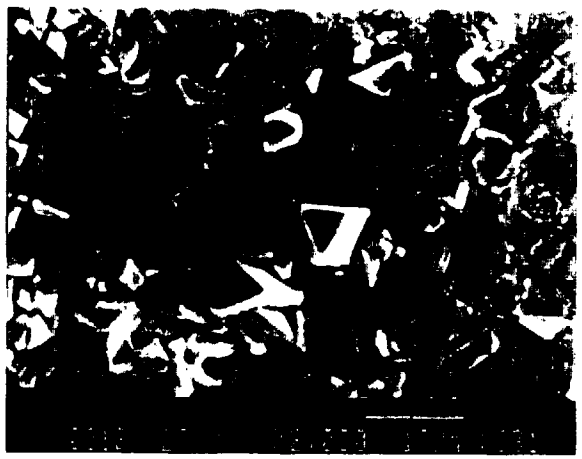

a)

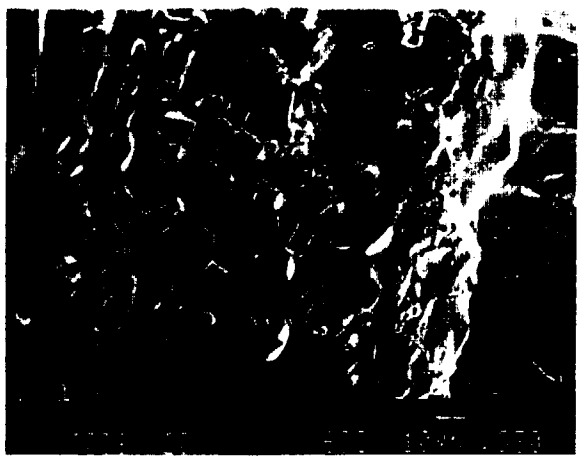

b)

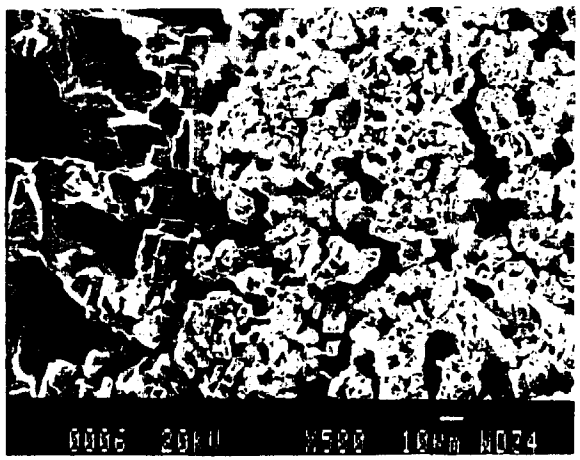

c)

Fig.5 a) Thorium crystals deposited on the cathode surface outside of the cathode spot. b) tungsten crystals deposited on the cathode surface outside of the cathode spot. c) tungsten crystals deposited near the necking area at the cathode spot.

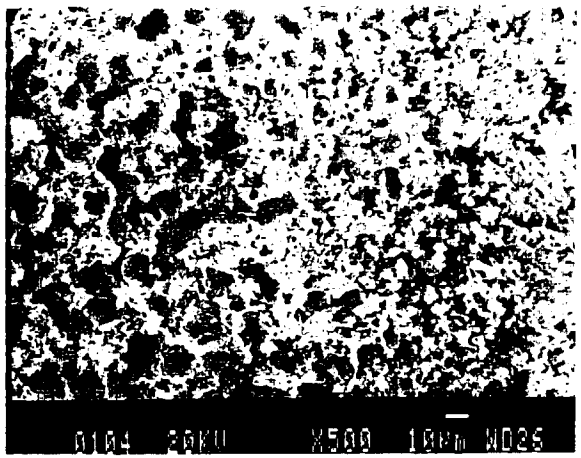

a)

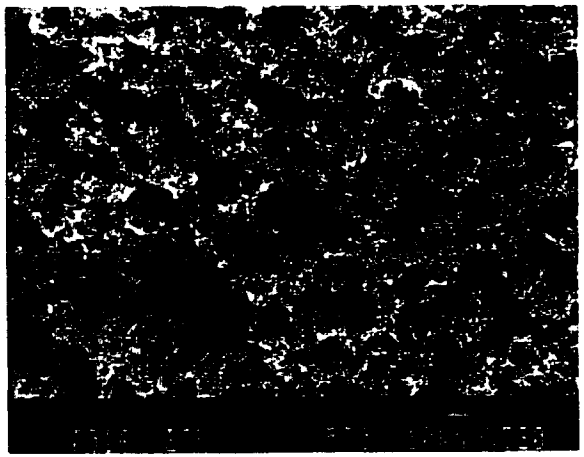

b)

c)

Fig.6 The porous cathode spot surface. a) after 5 minutes arcing. b) after 20 minutes arcing. c) after 60 minutes arcing.

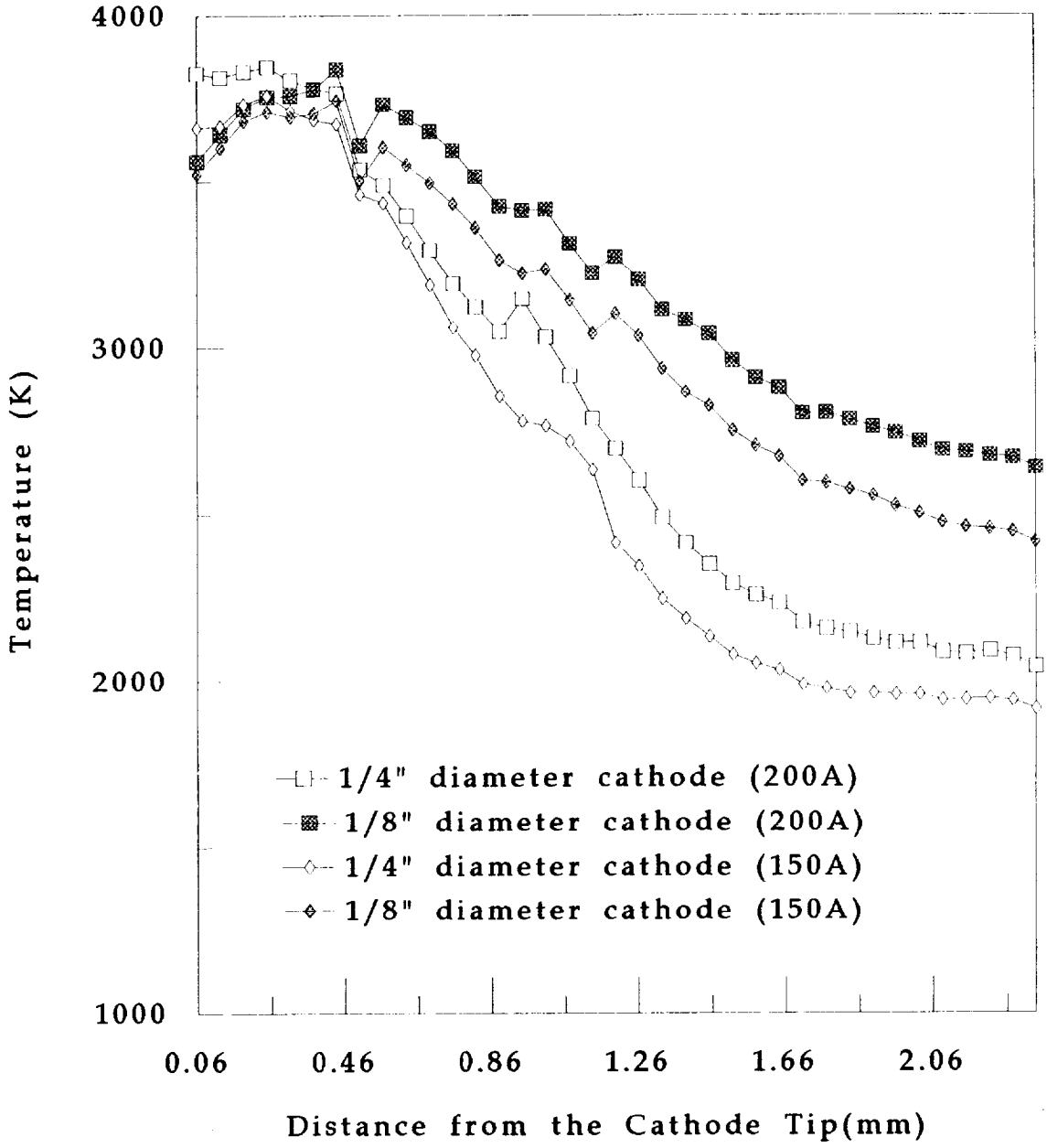

Fig.7 Cathode temperature distribution measured by OMA system using single color pyrometry

Figure 8. University of Minnesota Vacuum Facility

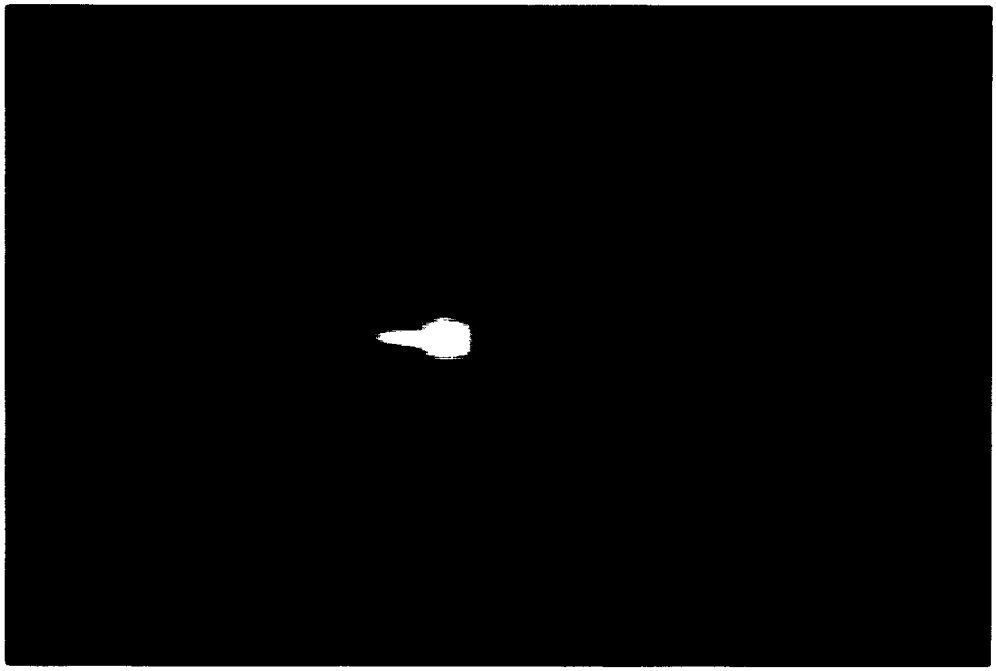

Figure 11. Low Power Arcjet in Operation

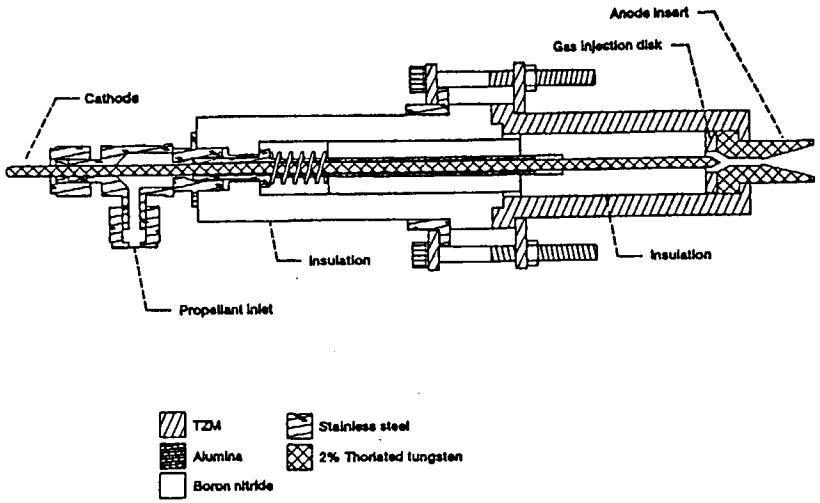

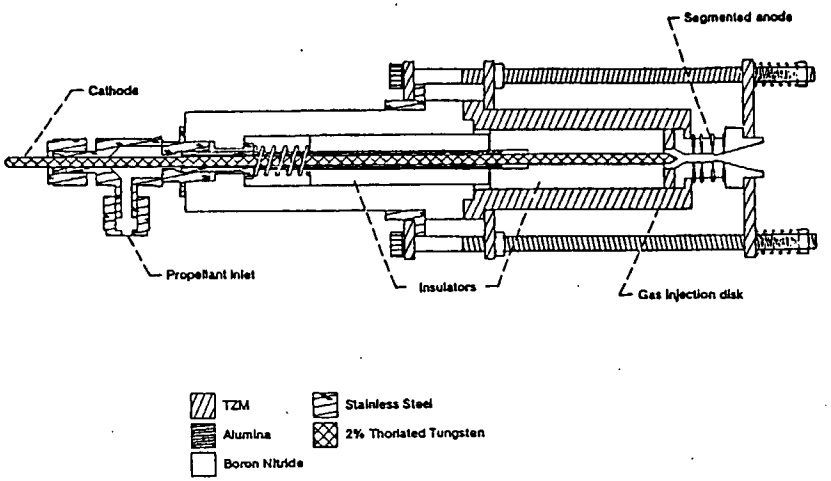

(a) Assembled Arcjet

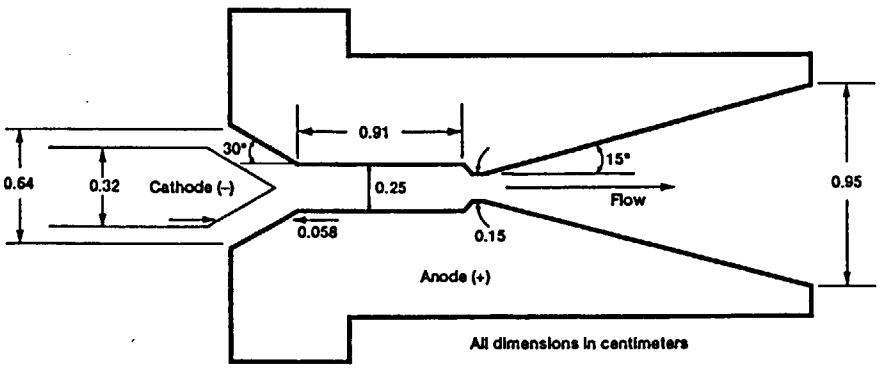

Figure 2.—Electrode geometry. (12)

(b) Solid Anode

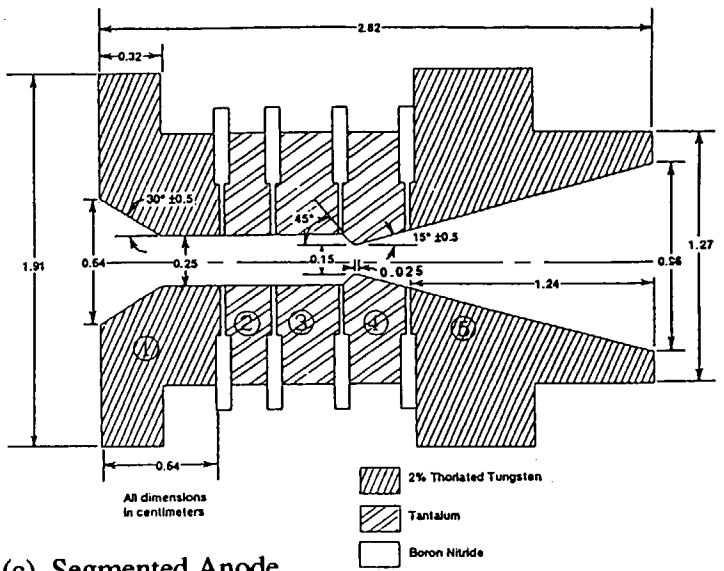

(c) Segmented Anode

Figure 9. Low Power Subsonic-Anode-Attachment Arcjet

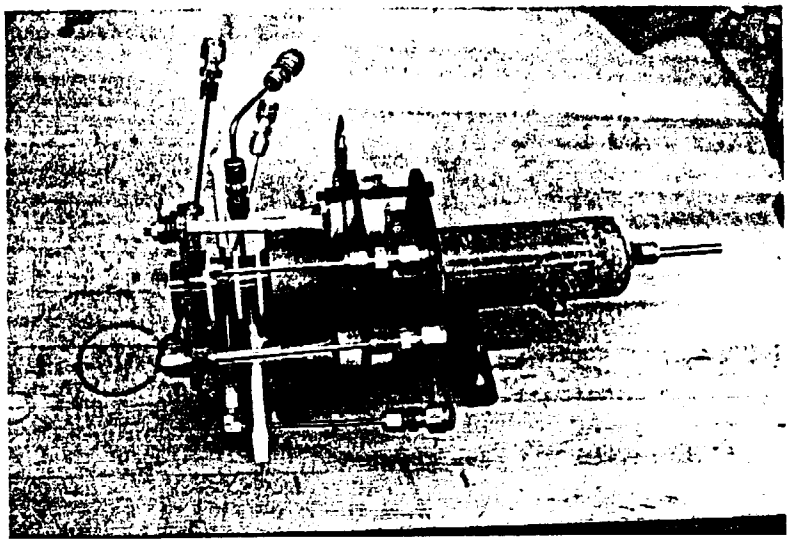

(a) Assembled Arcjet

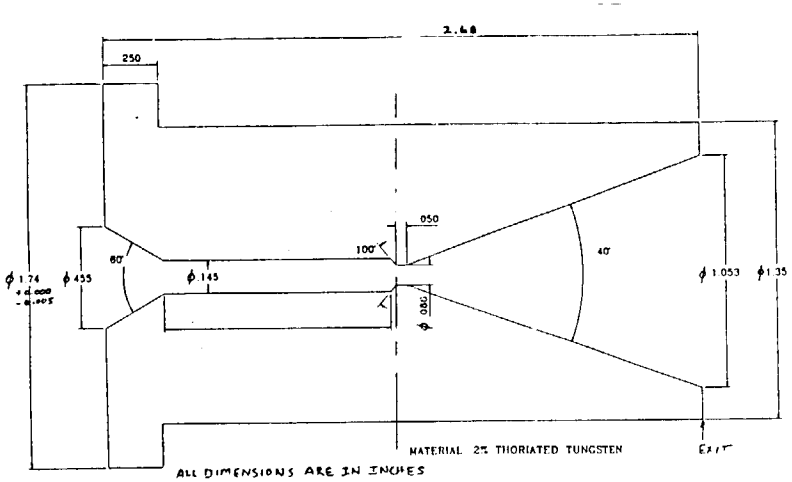

(b) Solid Anode

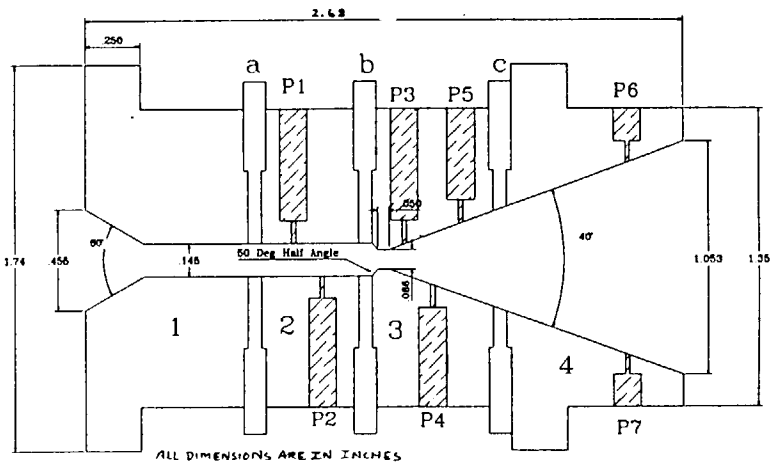

(c) Segmented Anode

Figure 10. Medium Power Subsonic-Anode-Attachment Arcjet

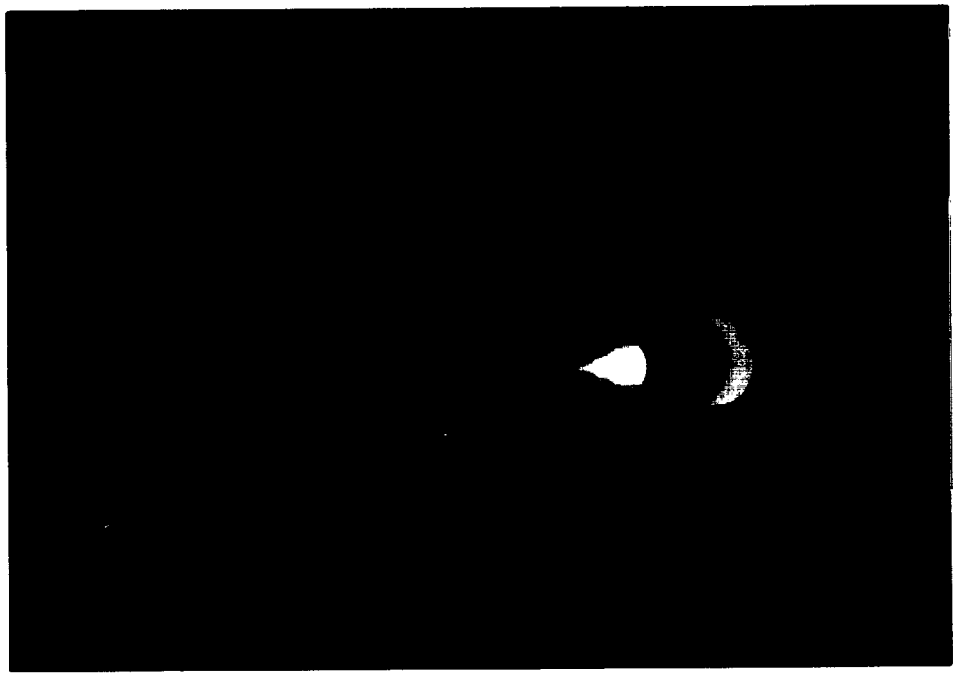

(a) Hydrogen, Tank Pressure ≈ 60 Torr

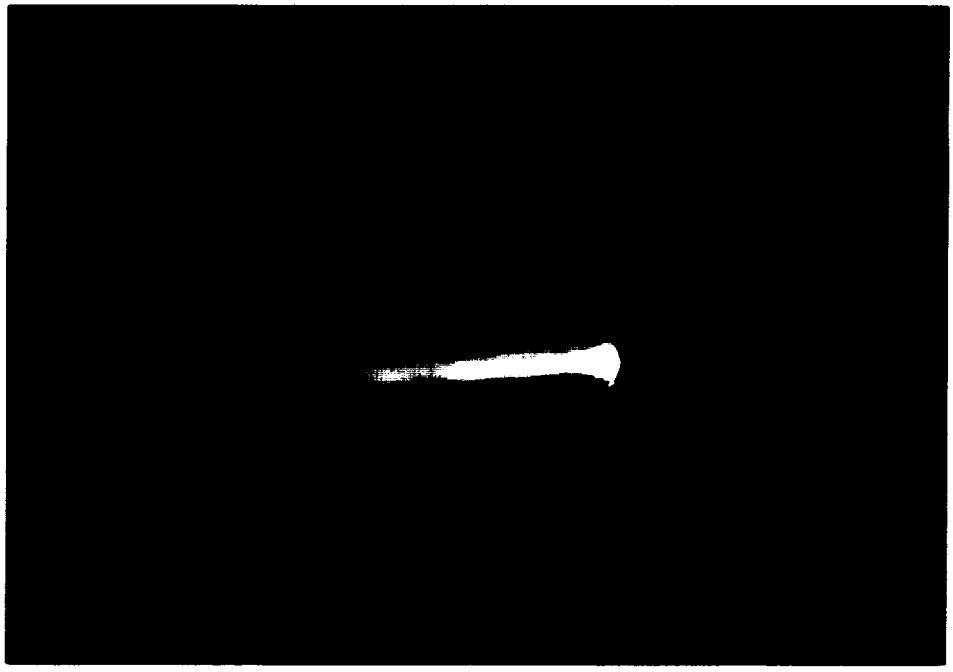

(b) Argon, Tank Pressure ≈ 60 Torr

Figure 12. Medium Power Arcjet in Operation

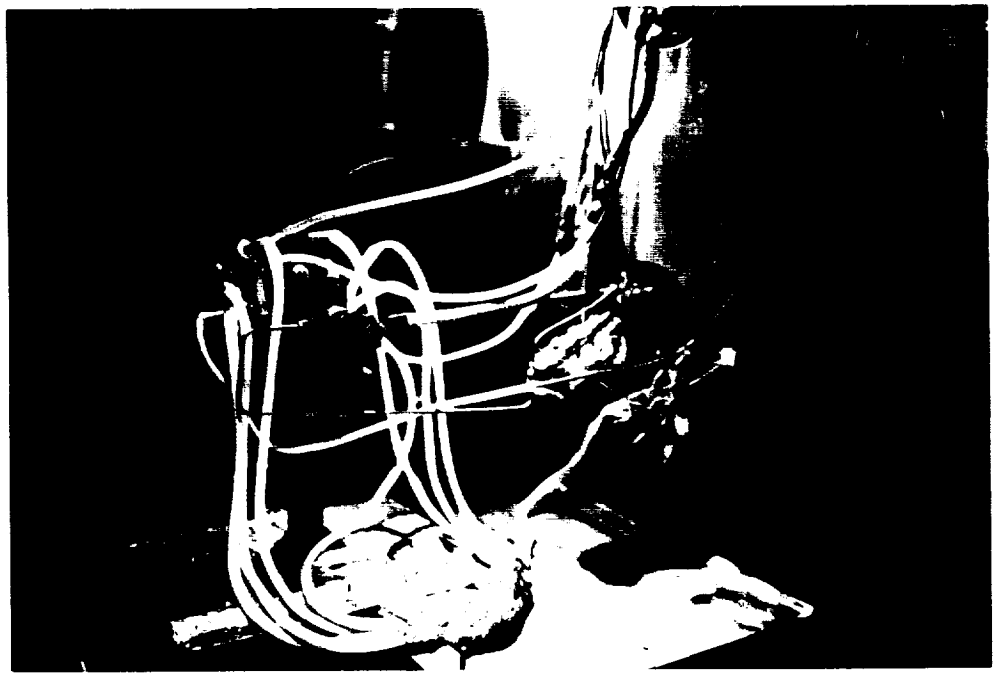

Figure 13. Medium Power Segmented Anode Arcjet Mounted in LeRC Tank 9

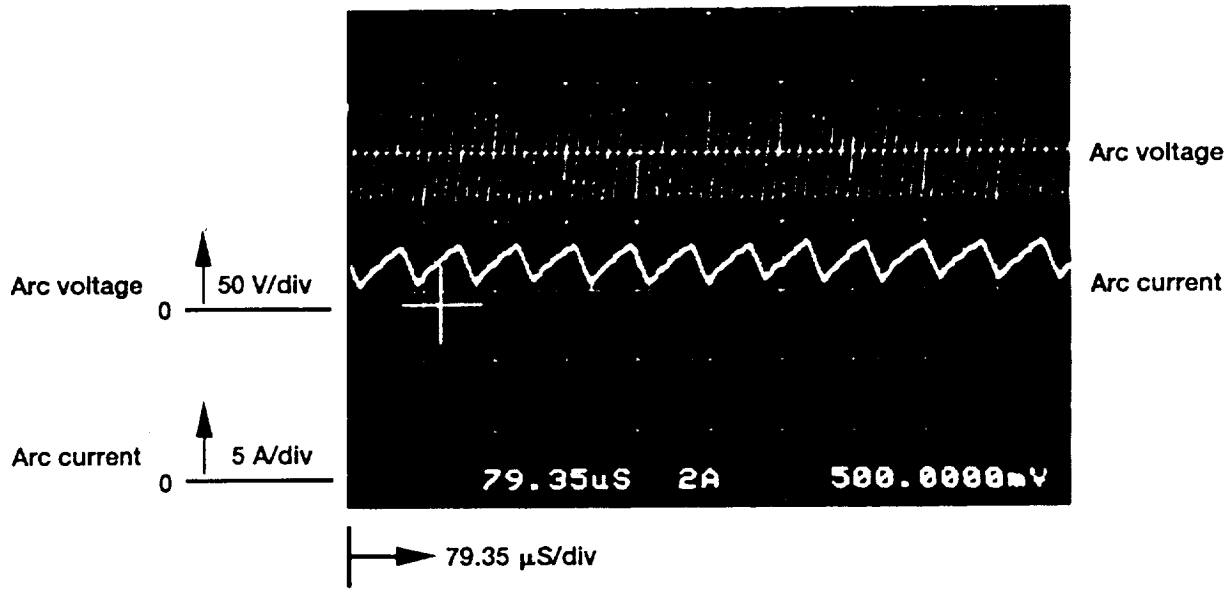

Figure 14. Oscilloscope Traces of Low Power Arcjet Voltage and Current, 30mg/s and 14A

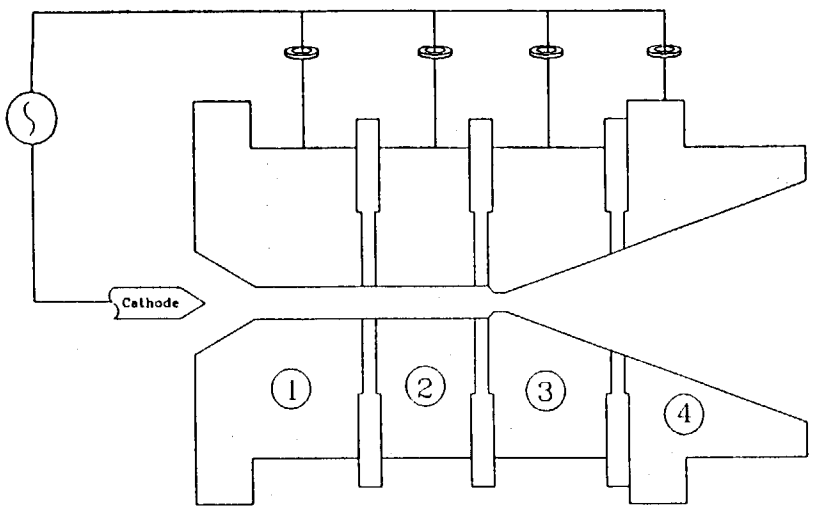

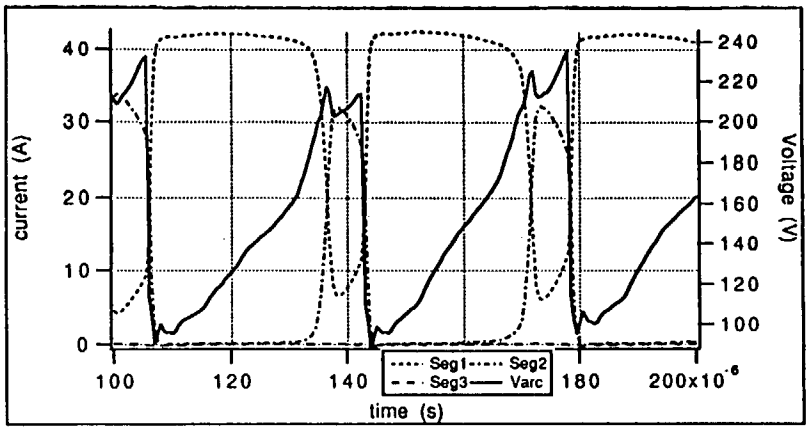

(a) 35 A, 79.7 mg/s

79.7 mg/s Constant

35 A - 166 V, 33203 Hz
40 A - 162 V, 37109 Hz
50 A - 156 V, 37109 Hz
55 A - 154 V, 41016 Hz

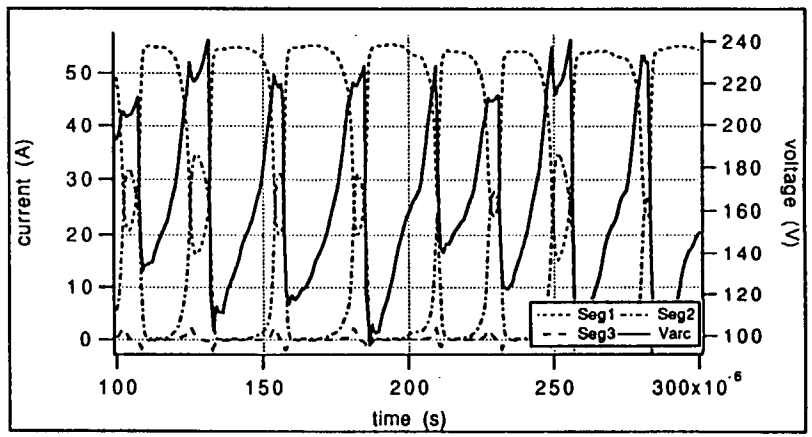

(d) 55 A, 79.7 mg/s

Figure 15. Oscilloscope Traces of Medium Power Segmented Anode Arcjet-
Constant flowrate of 79.7 mg/s and varying current

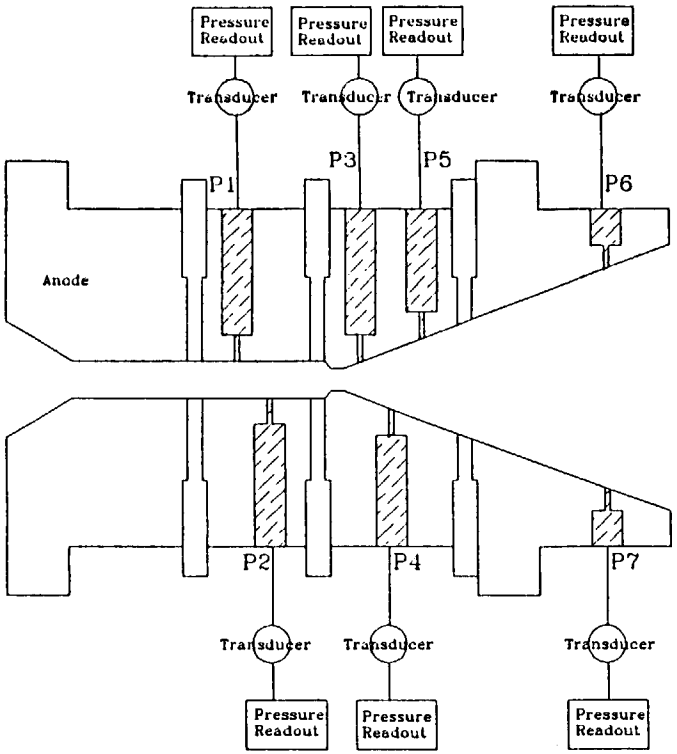

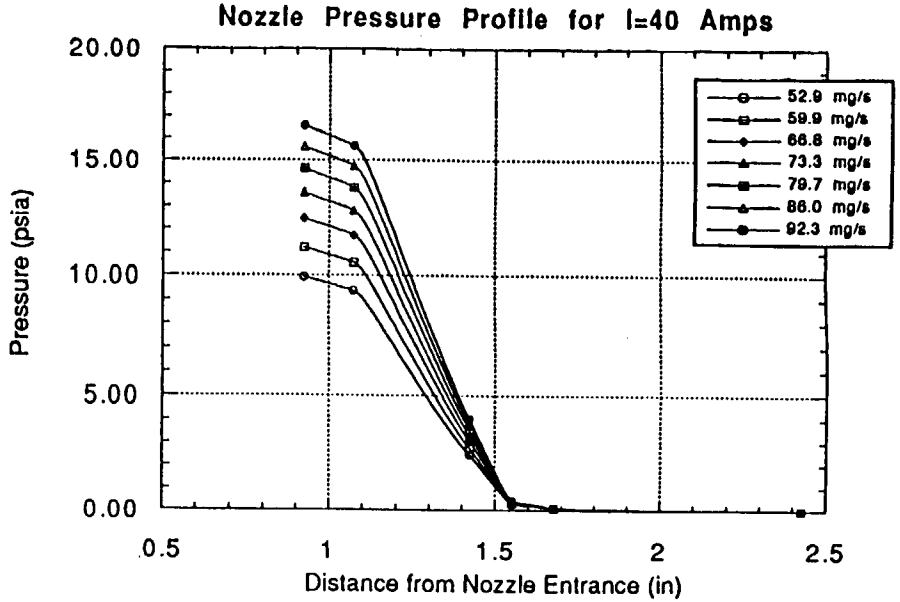

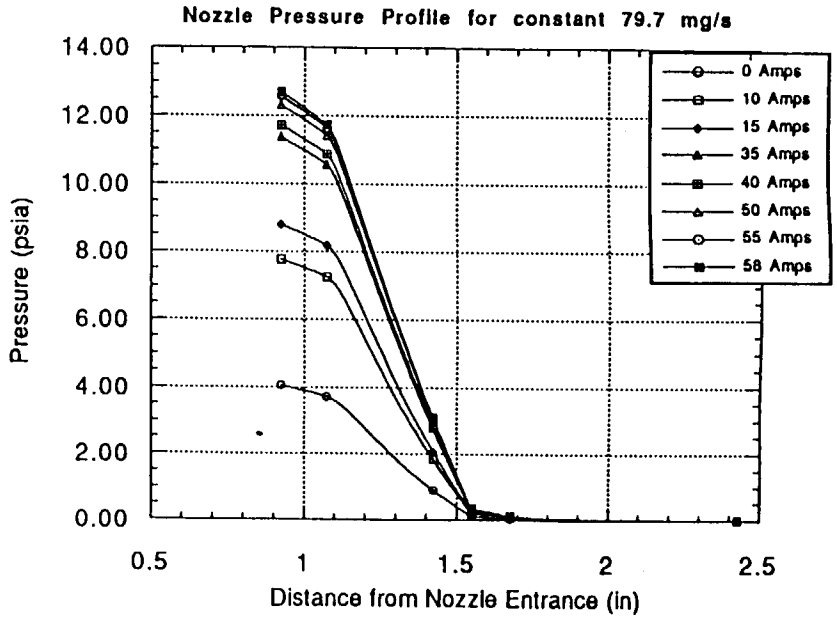

HEATED FLOW

Nozzle Pressure Profiles

Figure 16. Medium Power Arcjet - Nozzle Pressure Profiles for Constant Current and Constant Flowrate Operation